International Journal of Marine Engineering Innovation and Research, Vol. 9(2), June. 2024. 233-244
(pISSN: 2541-5972, eISSN: 2548-1479)

Failure Assessment of an In-service Pressure Vessel with Crack Flaw Using Failure Assessment Diagram

Wira Herucakra[1], Christina Dewi R.I. Simanjuntak[2]
(Received: 18 May 2024 / Revised: 20 May 2024 /Accepted: 26 May 2024)

***Abstract*— Failure assessment include fatigue assessment was performed for an in-service pressurize equipment utilized to support hydrocarbon proceesing activity as the response of crack-like flaw finding during phase array scanning inspection. The assessment required to ensure the integrity and the safety in the operation of deteriorated pressure vessel. The fitness-for-service assessment in this study are consist of failure assessment using Failure Assessment Diagram (FAD) and the fatigue assessment based on API 579-1/ASME FFS-1. The assessment has demonstrated that the current condition of the equipment was pass the assessment requirement and still has adequate strength and the fatigue damage due to actual operation pressure is an insignificant factor affecting the life of the equipment. This study also investigates the correlation between the geometry of the flaw and the stress increase ratio that is expressed in the exponential function as $\sigma C/\sigma R = 4.18e^{0.82(LD/T\hat{}2)}$**

Keywords— API RP 579-1/ASME FFS-1, Crack-liken flaw, Fitness-for-Service Assessment, Failure Assessment Diagram, Pressurized Equipment**.**

I. Introduction

A pressure vessel is a pressurized equipment for processing hydrocarbon from the initial separation, processing, condition treating, and storage with the common design and fabrication standard used is ASME Boiler and Pressure Vessel Code, Section VIII [1]. The pressurized vessels in the petroleum industry are such hazardous equipment, that degradation may occur within the service life of the equipment due to corrosion, mechanical damage, and other flaw that require to be maintained to avoid undesired catastrophic accidents. Furthermore, besides robust design and construction, the pressure vessel required to be inspected, monitored, and assessed periodically to ensure the integrity and safety of the equipment throughout the entire service life. American Petroleum Institute also provides guidance for the inspection, repair, and alteration of in-service pressurized equipment [2] and can be used in conjunction with the risk-based inspection recommended practice for better focus and effective in the prioritizing inspection planning [3].

During routine inspection using the ultrasonic scanning screening method, some in-service pressurized equipment was suspected to have a crack like flaw, and by the detailed inspection utilizing phase array ultrasonic thickness (Figure 1), the flaw was confirmed and the geometry was identified. failure assessment is then intended to be performed to ensure the integrity of equipment under deteriorated conditions for safety in operation and the fatigue assessment to estimate the residual life of the equipment.

Failure assessment through the Fitness for service (FFS) assessment Level 3 of crack-like flaw will be performed based on API 579-1/ASME FFS-1 Part 9 using the Failure Assessment Diagram (FAD) method as an early assessment to understand the behavior of the flaw under actual operating conditions, whether the deterioration condition is within acceptable criteria and the flaw categorized as non-crack growth or the flaw having potential to growth and required further advanced evaluation. Fatigue Assessment was also performed to estimate the life of equipment based on API 579-1/ASME FFS-1 Part 14 [4]. A similar case was discussed by Ghanbari as a discontinuity finding at a pressurize gas separator vessel by Phase Array Ultrasonic Testing (PAUT) device, the numerical 3D simulation, and the fitness for service assessment using failure analysis diagram (FAD) method based on API 579 was performed to evaluate hydrogen-induced crack [5].

The first edition of API Recommended Practice 579 was developed and introduced in the 2000 by American Petroleum Institute and The American Society of Mechanical Engineers [6]. This standard provides guidance on the assessment of deteriorated in-service pressurized equipment with a wide range of damage mechanisms that are not addressed in the design code, including The Failure Assessment Diagram (FAD) method for evaluating crack-like flaws that similar to British Energy and the British Standard Institute method [7]. The API 579 third edition and above provide additional guidance related to fatigue assessment with a multi-tiered approach and cycle counting method for both welded joint and smooth bar fatigue methods [8].

Fitness for service assessment using FAD method has been widely applied in for pressurized equipment, they

Wira Herucakra, PT Dinamika Teknik Persada, South Tangerang, 15139, Indonesia. E-mail: wira.herucakra@dtp-eng.com
Christina Dewi R.I. Simanjuntak, PT Dinamika Teknik Persada, South Tangerang, 15139, Indonesia. E-mail: christina@dtp-eng.com

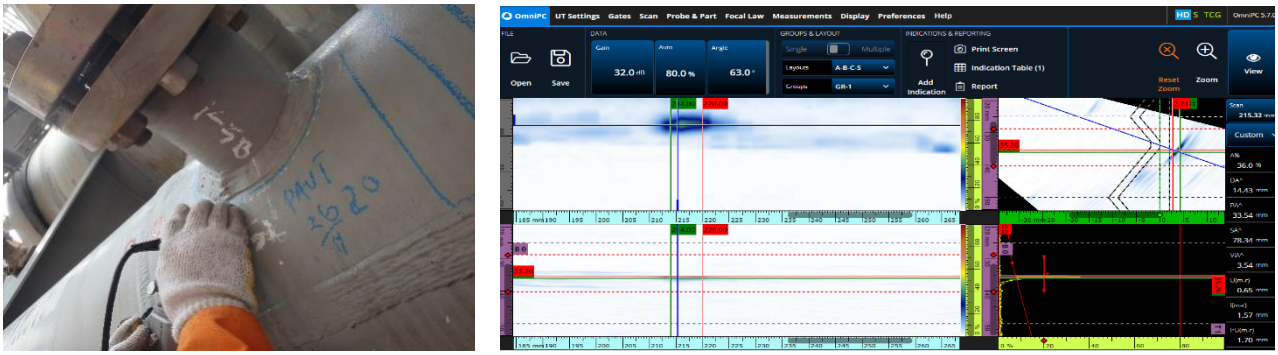

Figure. 1. Phase array ultrasonic testing (PAUT) inspection activity (case no. 4.1 and 4.2, see table 4)

are, weld crack assessment for the hydrocarbon pipeline with material grade of API X65 [9], structural integrity assessment through the experimental and numerical analysis for axially cracked pipelines [10], Experimental and numerical analysis to estimate pressure failure of cracked composed natural gas cylinder [11], Structural Integrity analysis of steam generator turbine in nuclear power plan with varied crack geometries and loading condition [12], Failure assessment on the cracked pressurize piping considering random and fuzzy uncertainties [13], failure assessment of piping on nuclear power plan contain defect at straight and elbows [14], Assessment for 70 km gas pipeline with corrosion defect based on magnetic flux leaked (MFL) intelligent pig tools data [15], assessment of steel pipeline made of API 5L X52 with corroded at elbow [16].

The Failure assessment diagram method is not limited applicable for steel walled pressured equipment problem, several non-pressurized equipment problem that was assessed using FAD method, they are, FAD use to estimate the initiating of brittle fracture at the end of structural CJP groove welded joint with defect due to post earthquake Kobe 1995 [17], failure assessment structural square hollow section with crack at T-joint [18], validation of BS7910:2005 assessment procedure for structural square hollow section with crack at T-, Y- and K-Joints [19], failure assessment of cracked X and K joints of structural circular hollow section [20], study on development of deformation limit using FAD method for fatigue-cracked X-joint of structural hollow section subjected in-plane flexure [21], Extensive assessment of notched structural steel component [22], Assessment of aero-engine turbine disk beyond normal operation condition [23], an extensive failure and fatigue assessment for component subjected with rolling contact using FAD method with varies variable [24]. Non-steel walled equipment that was assessed using FAD method, they are, Failure assessment on Zr-2.5Nb alloy material pressure tube used in the Canadian Deuterium Uranium (CANDU) heavy water reactor due to delayed hydride cracking [25], failure assessment for 316H stainless steel containing creep crack [26], assessment of Ti-6Al-4V titanium alloy laser welded plate containing undercut defect [27], fracture assessment of notched short glass fibre reinforced polyamide 6 (SGFR-PA6) [28], failure assessment of nuclear steam generator tubes (SGTs) made of Inconel 690 and incoloy 800 [29], extensive assessment of additively manufactured (AM) specimen containing noctes [30], strength analysis of lithium hydride ceramic subjected thermal stresses during sintering process [31].

II. METHOD

The API Recommended Practice 579-1/ASME FFS-1 Part 9 covers the fitness for service (FFS) assessment procedure used to evaluate crack-like flaws in components. The assessment procedure is based on the Failure Assessment Diagram (FAD) Method, which is summarized in Figure 2. The stress analysis concepts and methods used in the API Recommended Practice 579-1/ASME FFS-1 Part 9 are based on ASME B&PV Code, Section VIII, Division 2 (VIII-2), part 5.

A. *Flaw Characterization*

The characterization of crack flaws is ruled in the API 579-1/ASME FFS-1 Section 9.3.6 for simplification of the actual crack geometry model and to make more amenable fracture mechanic analysis. The rule has accounted for flaw shape, orientation, and interaction that was tailored to characterize crack-like to lead idealized models that are more severe than actual geometry.

The mesh design technique adopted in this paper refers to the guideline provided by Anderson based on the crack plane model of a two-dimensional problem using the quadrilateral element with focused “spider web” mesh concentrated at the crack tip as illustrated in Figure 3 [32].

As idealized geometry was obtained, the finite element model was then developed. Figure 4 presents of developed crack plane two-dimensional finite element model for embedded flaw taken form case no 5.1 to 5.3 (See Table 4). and the surface flaw model taken form case no. 1.1 to 1.2 (See Table 4).

B. *Fitness-for-Service Assessment Crack-Like Flaw*

The level 3 assessment procedure provides the best estimate of the structural integrity of a component crack-like flaw. The level 3 assessment that will be used in this

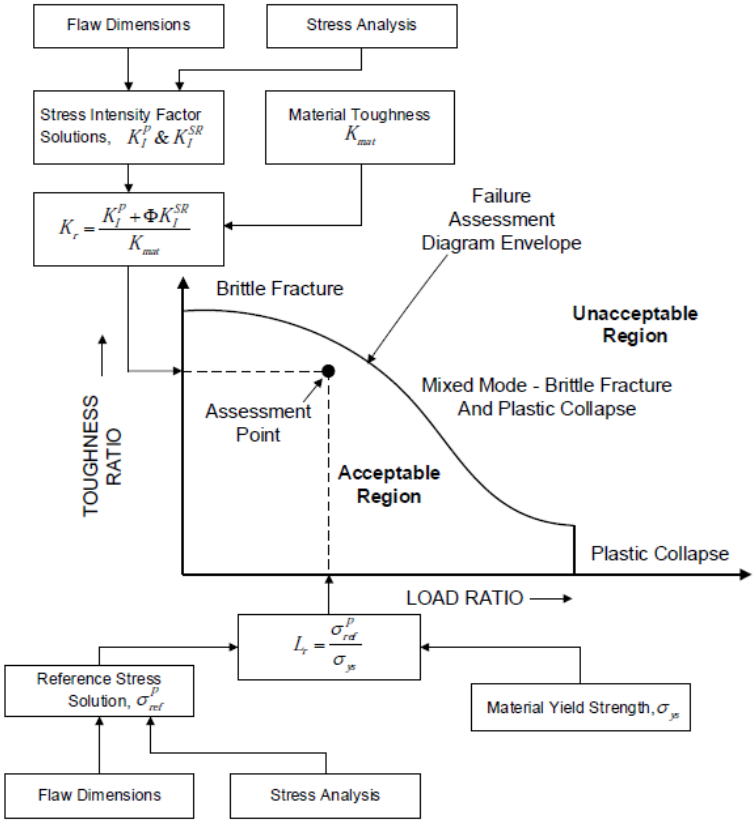

Figure. 2. Overview of failure assessment diagram (FAD) method [4]

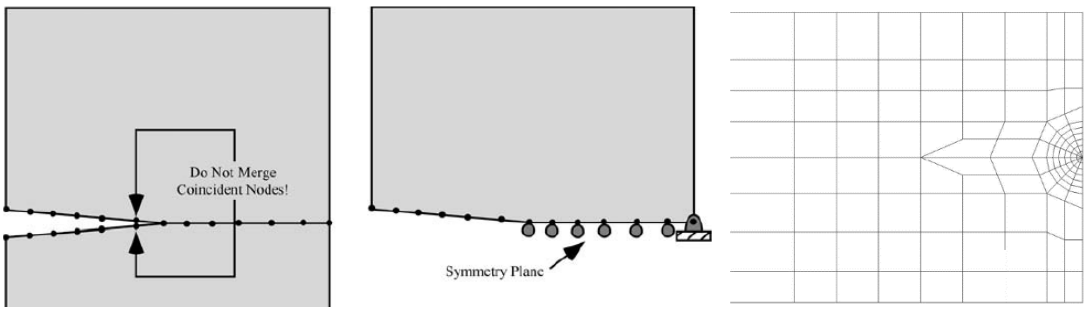

Figure. 3. Boundary and focused mesh design model for crack plane of two-dimensional finite element problem [32]

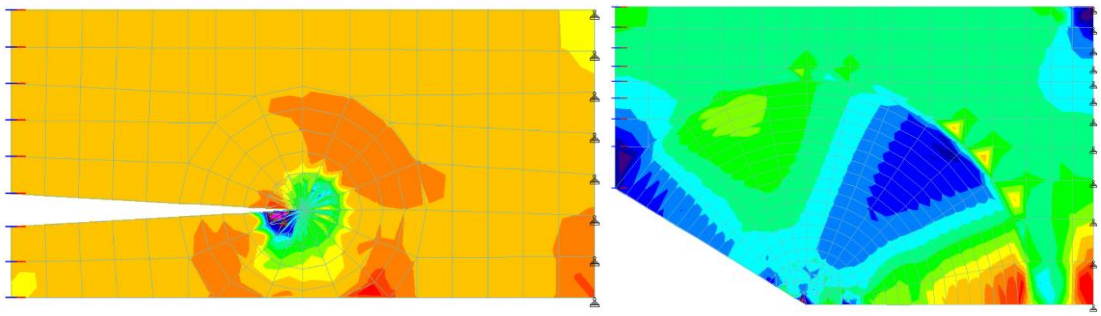

Figure. 4. Two-dimensional finite element model. Left: embedded flaw (case no. 5.1 to 5.3, see Table 4), Right: surface flaw (case no. 1.1 and 1.2, see Table 4)

study is based on API Method A Assessment as discussed in the 579-1/ASME FFS-1 Section 9.4.4.1 point a. As illustrated in Figure 2, the toughness ratio, K_r, is expressed as:

$$K_r = \frac{K_I}{K_{mat}} \quad (1)$$

where K_I is stress intensity attributed to the primary loads using primary stress distribution, and K_{mat} is material toughness. K_{mat} applied for the analysis is 129.37 MPa m0.5 refer to the experimental result performed by Vishal that evaluate fracture parameter for SA-516 Grade 70 material [33]. K_I is defined as:

$$K_I = 1.12\sigma_{ref}^{P}\sqrt{\pi a} \quad (2)$$

The load ratio, L_r^P, is expressed in the following equation:

$$L_r^P = \frac{\sigma_{ref}^{P}}{\sigma_{ys}} \quad (3)$$

where σ_{ref}^{P} is the reference primary stress and σ_{ys} is yield strength of material. If the result of the assessment falls inside the FAD curve, the result is acceptable and the unstable crack growth will not occur. If the result of the assessment fall outside the FAD and subsequent point fall within the FAD, then the few amounts of crack growth or stable ductile tearing will occur. Ductile instability estimated when the result of the assessment fall outside the FAD. The FAD curve is expressed as follow:

$$K_r = \left[\begin{matrix}(1 - 0.14(L_r^P)^2) + \\ (0.3 + 0.7exp[-0.65(L_r^P)^6])\end{matrix}\right] \quad (4)$$

C. *Fatigue Assesment*

The Assessment of Fatigue Damage Level 2 was used in this paper, the procedure as mentioned in the API Recommended Practice 579-1/ASME FFS-1 Part 14. Method A: fatigue assessment using elastic stress analysis and equivalent stress is selected in this case. In this method, the fatigue damage is computed based on effective total equivalent stress obtained from linear elastic stress analysis, and a smooth bar fatigue curve. The procedure fatigue assessment is referred to the steps that are summarized in Figure 5.

The equivalent stress range, $\Delta S_{P,k}$, within step no. 4.2 are experessed as:

$$\Delta S_{P,k} = \frac{1}{\sqrt{2}}\left[\begin{matrix}\left(\Delta\sigma_{11,k} - \Delta\sigma_{22,k}\right)^2 + \\ \left(\Delta\sigma_{11,k} - \Delta\sigma_{33,k}\right)^2 + \\ \left(\Delta\sigma_{22,k} - \Delta\sigma_{33,k}\right)^2 + \\ 6\left(\Delta\sigma_{12,k}^2 + \Delta\sigma_{13,k}^2 + \Delta\sigma_{23,k}^2\right)\end{matrix}\right]^{0.5} \quad (5)$$

where $\sigma_{ij,k}^{m}$ is Stress tensor at the location under evaluation at the point t^m for the k^{th} cycle, and $\sigma_{ij,k}^{n}$ is the stress tensor at the location under evaluation at the point t^n for the k^{th} cycle

The effective alternating equivalent stress amplitude, $S_{alt,k}$, within step no. 4.3 are expressed as:

$$S_{alt,k} = \frac{K_{e,k}\Delta S_{P,k}}{2} \quad (6)$$

where the fatigue penalty factor, $K_{e,k}$ evaluated based on the following condition.

a. for $(S_{n,k} \le S_{PS})$, $K_{e,k} = 1.0$
b. for $(S_{PS} \le \Delta S_{n,k} \le mS_{PS})$, $K_{e,k}$, refer to the following equation

$$K_{e,k} = 1.0 + \frac{(1-n)}{n(m-1)}\left(\frac{\Delta S_{n,k}}{S_{PS}} - 1\right) \quad (7)$$

c. for $(\Delta S_{n,k} \ge mS_{PS})$, $K_{e,k} = {}^{1}/_{n}$

where $\Delta S_{n,k}$ is the primary plus secondary equivalent stress range and S_{PS} is the Allowable limit on the primary plus secondary stress range and the parameter *m* and *n* are determined from the table 1.

Once the alternating equivalent stress amplitude, $S_{alt,k}$, computed, the permissible number of cycles, N_k, can be determined using fatigue curve for carbon for temperature not exceeding 700°F and the ultimate tensile strength not exceeding 80 ksi is selected to determine the permissible number of cycles as presented in the figure 6.

Fatigue damage, $D_{f,k}$, and accumulated fatigue damage, D_f, can be calculated based on equation (8) and (9) respectively as follow:

$$D_{f,k} = \frac{n_k}{N_k} \quad (8)$$

$$D_f = \sum_{k=1}^{M} D_{f,k} \le 1.0 \quad (9)$$

Where n_k is the actual number of the k^{th}cycle.

III. RESULT

A. *Equipment Description*

Based on the previous inspection, the inspection result found some flaw discontinuity on the pressure vessel nozzle. A Fitness for Service (FFS) assessment is required to be performed based on API 579. The general data of pressured equipment to be considered in the assessment are listed in Table 2. The actual crack flaw geometry recorded from the phased array UT inspection and then conservatively idealized based on the rule on API 579-1/ASME FFS-1 Section 9.3.6 are presented in Table 3.

Actual operating pressure records for each piece of equipment are presented in Figure 7. Based on the

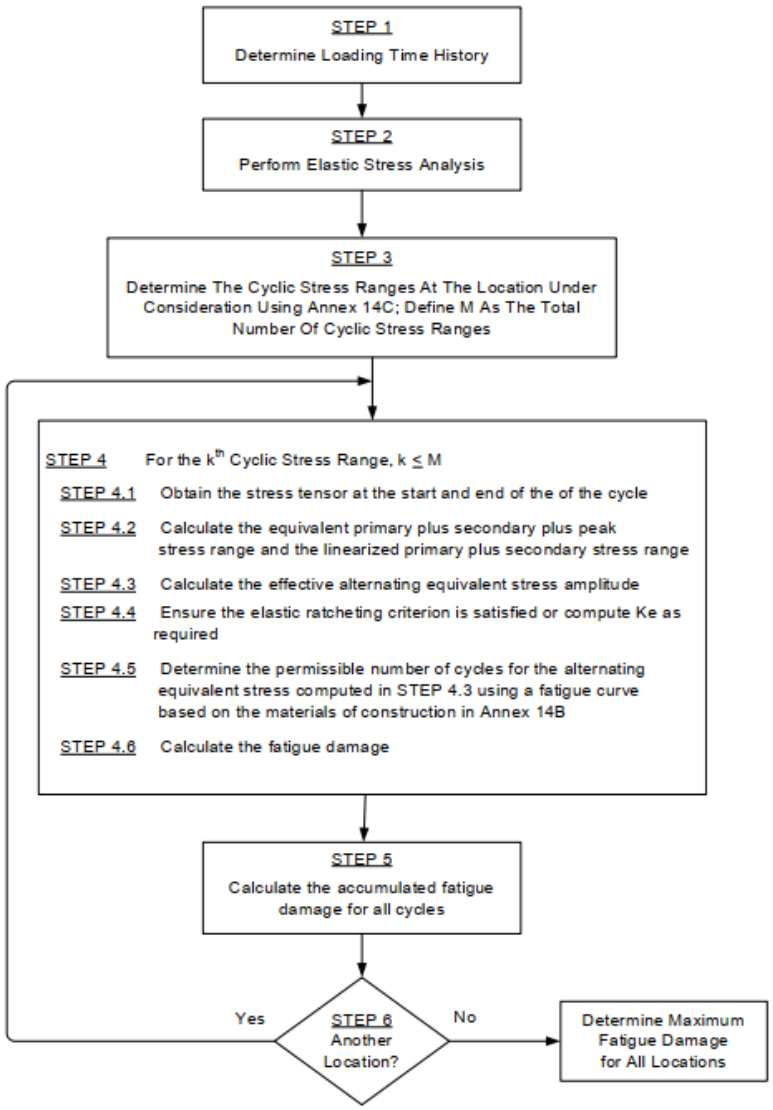

Figure. 5. Fatigue Assessment Level 2 Method A (API 579, 2021)

TABLE. 1. FATIGUE PENALTY FACTOR (API 579, 2021)

Material	$K_{e,k}$ (1)		$T_{max,k}$ (2)	
	m	n	(°C)	(°F)
Low alloy steel	2.0	0.2	371	700
Martensitic stainless steel	2.0	0.2	371	700
Carbon steel	3.0	0.2	371	700
Austenitic stainless steel	1.7	0.3	427	800
Nickel-chromium-iron	1.7	0.3	427	800
Nickel-copper	1.7	0.3	427	800

Notes:
1. Fatigue penalty factor.
2. The fatigue penalty factor should only be used if all of the following are satisfied:
   - The component is not subject to thermal ratcheting, and
   - The maximum temperature in the cycle is within the value in the table for the material.

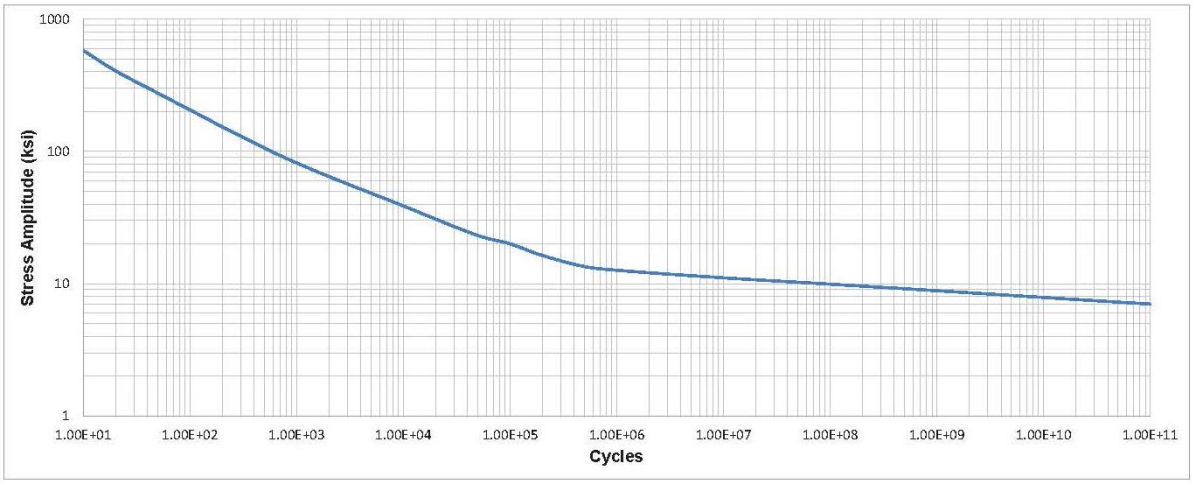

Figure. 6. Fatigue curve for carbon low alloy, series 4XX, high alloy steel and high tensile strength for temperature not exceeding 700° - σuts < 80 ksi (API 579, 2021)

TABLE. 2. GENERAL DATA OF EQUIPMENT

Tag ID	PV-01	PV-02	PV-03	PV-04
Name	Slug Catcher Inlet Separator	Production Separator	Amine Contactor Inlet KO Drum	Amine Contactor
Picture				
Type	Horizontal	Vertical	Horizontal	Vertical
MAWP	1023.97 psig	1020.92 psig	1041.08 psig	1027.74 psig
Operating Pressure	507.63 psig	493.12 psig	493.12 psig	435.11 psig to 580.15 psig
Diam ID.	59.06 inch	48.03 inch	41.008 inch	105.12 inch
Length	15.75 feet	16.33 feet	8.67 feet	42.35 feet
Shell Nom. Thk.	1.89 inch	1.46 inch	1.5 inch	2.72
Corrosion allowance	0.24 inch	0.118 inch	0.118 inch	N/A
Shell Material	A-516 Gr 70N	A-516 Gr 70N	A-516 Gr 70N	A-516 Gr 60N
Yield strength	260 Mpa	260 Mpa	260 Mpa	250 Mpa
Tensile strength	485-620 Mpa	485-620 Mpa	485-620 Mpa	415-550 Mpa
Age	15 years	15 years	15 years	15 years

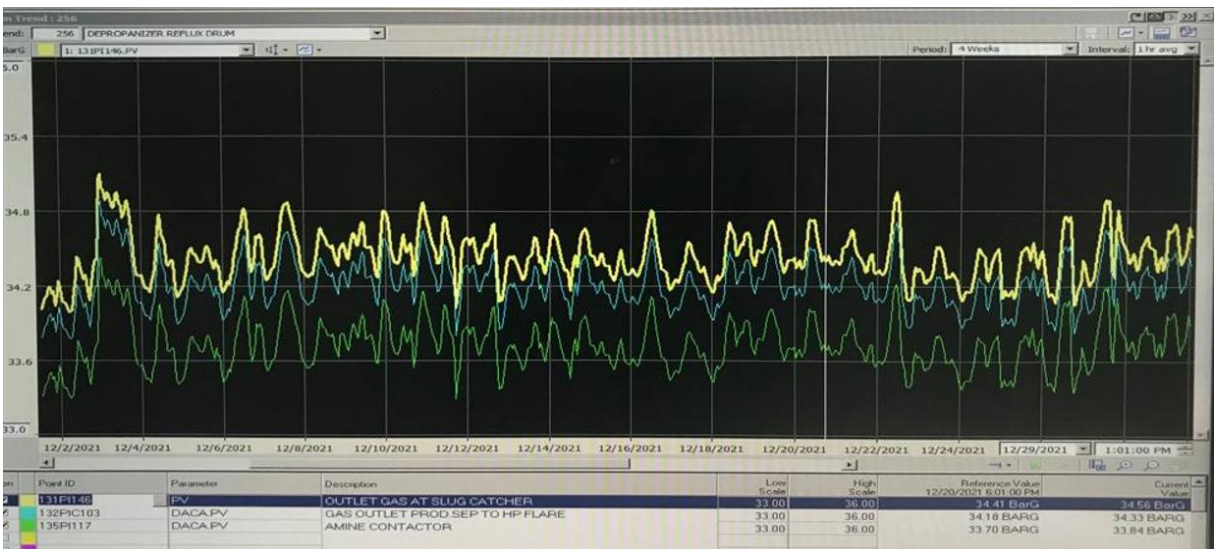

Figure. 7. Record of actual operating pressure

TABLE. 3. CRACK GEOMETRY MODEL IDEALIZATION

Case	Actual geometry	Idealization	Flaw geometry idealization
PV-01 Slug Catcher Inlet Separator Nozzle N1 t = 47.5 mm	Embedded flaw 1 d_1 = 28.87 mm d_2 = 33.88 mm a_1 = 25.05 mm depth = 5.01 mm Embedded flaw 2 d_1 = 37.37 mm d_2 = 45.75 mm a_2 = 4.19 mm depth = 8.38 mm Length flaw 1 and 2 = 58 mm Offset = 6 mm S_1 = 3.49 mm S_2 = 0.00 mm	$S_1 \leq$ max (a1, a2) 3.49 mm $\leq$ 4.19 mm → Interaction of two Embedded flaw Combined flaw d_1 = 28.87 mm d_2 = 45.75 mm depth = 16.88 mm Length = 61.5 mm (18°: 6-9 o/c) d_2/t = 0.03 $\leq$ 0.2 → surface flaw Length = 61.5 mm Depth = 18.63 mm	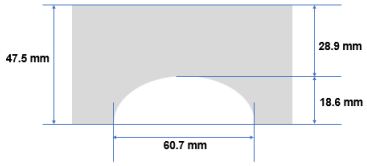
PV-01 Slug Catcher Inlet Separator Nozzle N5 t = 47.5 mm	Embedded flaw d_1 = 28.89 mm d_2 = 40.81 mm depth = 11.92 mm Length = 148 mm (43°: 6-9 o/c) Offset = 6 mm	d_2/t = 0.14 $\leq$ 0.2 → surface flaw Length = 131 mm Depth = 11.9 mm	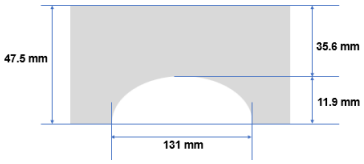
PV-02 Production Separator Nozzle N4 t=37 mm	Embedded flaw d_1 = 11.83 mm d_2 = 15.60 mm depth = 3.77 mm length = 10.18 mm (18.2°: 12-5 o/c) offset = 12.96 mm	d_1/t = 0.3 $\geq$ 0.2 → Embedded flaw	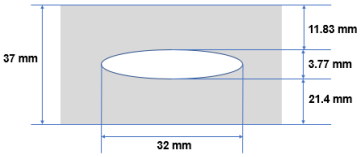
PV-03 Amine Contactor Inlet KO Drum Nozzle K5B t = 25 mm	Embedded flaw d_1 = 21.53 mm d_2 = 24.04 mm depth = 2.5 mm length = 29 mm offset = 3 mm	d_2/t = 0.03 $\leq$ 0.2 → surface flaw Length = 30.92 mm (22.4°: 9-12 o/c) Depth = 3.46 mm	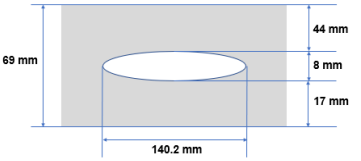
PV-04 Amine Contactor Nozzle N4A t = 69 mm	Embedded flaw d_1= 44 mm d_2 = 52 mm depth = 8 mm length = 218 mm (91.6°: 9-12 o/c) offset = 11 mm	d_2/t = 0.3 $\geq$ 0.2 → Embedded flaw	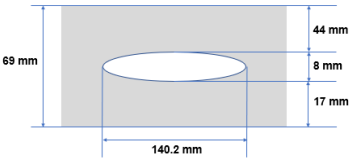
PV-04 Amine Contactor Nozzle N4C t = 69 mm	Embedded flaw d_1 = 52 mm d_2 = 57 mm Depth = 5 mm Length = 73 mm Offset = 4 mm	d_2/t = 0.17 $\leq$ 0.2 → surface flaw Length = 103 mm (45.6°: 6-9 o/c) Depth = 17 mm	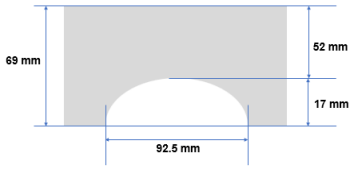

Note:
t = shell thickness; d_1= distance between edge of flaw to inner side of shell plate; d_2 = distance between edge of flaw to outter side (surface)of shell plate; a_1 = half depth of first flaw; a_2 = half depth of second flaw; s_1=tranverse distance between two flaw; s_2= longitudinal distance between two flaw

recorded data, the actual operating pressure is far below the Maximum Allowable Working Pressure (MAWP), this fluctuates between a range of 49 to 56 percent of the MAWP.

B. *Failure Assessment Diagram (FAD) Result*

The result of the Fitness for Service Assessment for crack flaw through the FAD method is summarized in Table 4 and plotted along the Fracture Assessment Diagram as presented in Figure 8.

As discussed in Section 3.1 previously, the actual operating pressure recorded is about 49 to 56 percent below the Maximum Allowable Working Pressure, hence, based on the FAD assessment result as summarized in Table 4. Generally, the current deteriorated condition of pressure vessel equipment has adequate strength under operating pressure. Furthermore, as the actual operating pressure value is below the FAD curve, the existing flaw is not caused by operating conditions but is suspected to have existed within the construction phase.

C. *Fatigue Assessment*

Results of fatigue assessment for crack flaw condition are summarized in Table 5. Generally, the alternating stress, S_{ALT}, produced from fatigue load is below the threshold line of the SN Curve (about 7 ksi) resulting in the estimated allowable fatigue cycle for all equipment being over 1.00 x 10^{10} cycle or can be considered as infinite condition.

TABLE. 4. FAD CALCULATION SUMMARY

#	Case	Condition	Pressure psig	σPref Mpa	LPr -	KI Mpa m0.5	Kr -	Remark
1.1	PV-01 Slug Catcher Inlet Separator Nozzle N1	MAWP	1023.97	28.883	0.11	9.986	0.08	acceptable
1.2		OP	507.63	14.303	0.06	4.945	0.04	acceptable
2.1	PV-01 Slug Catcher Nozzle N4	MAWP	1023.97	46.106	0.18	23.419	0.18	acceptable
2.2		OP	507.63	22.828	0.09	11.595	0.09	acceptable
3.1	PV-02 Prod. Separator Nozzle N1	MAWP	1020.92	12.121	0.05	3.043	0.02	acceptable
3.2		OP	493.12	6.026	0.02	1.513	0.01	acceptable
4.1	PV-03 Amine Contactor Inlet KO Drum Nozzle K5B	MAWP	1041.08	27.099	0.10	6.609	0.05	acceptable
4.2		OP	493.12	13.211	0.05	3.222	0.02	acceptable
5.1	PV-04 Amine Contactor Nozzle N4A	MAWP	1027.74	213.921	0.82	112.408	0.87	Unacceptable
5.2		OP	677.33	140.986	0.54	74.083	0.57	Acceptable
5.3		OP	580.15	120.758	0.46	63.454	0.49	Acceptable
5.3		OP	507.63	105.668	0.40	55.525	0.43	Acceptable
6.1	PV-04 Amine Contactor Nozzle N4C	MAWP	1027.74	38.673	0.15	16.506	0.13	Acceptable
6.2		OP	677.33	25.488	0.10	10.879	0.08	Acceptable
6.3		OP	580.15	21.830	0.08	9.317	0.07	Acceptable
6.4		OP	507.63	19.100	0.07	8.152	0.06	Acceptable

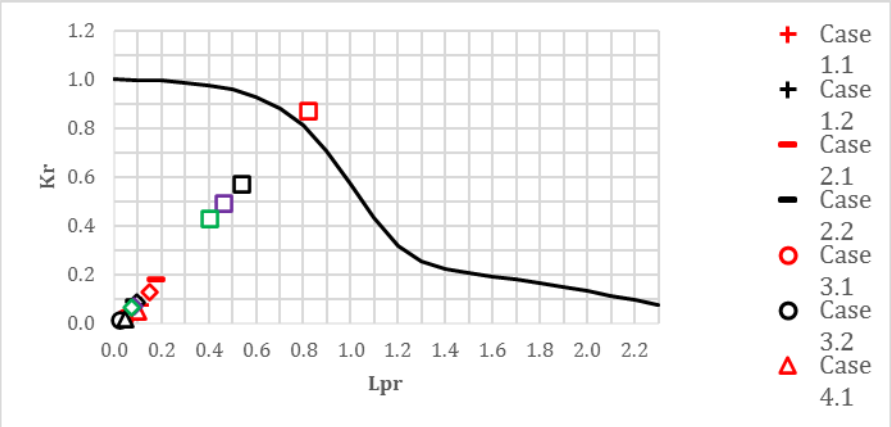

Figure. 8. Plotted result of FAD calculation

TABLE. 5. FATIGUE ASSESSMENT RESULT

Case	Op. Pressure bar	Occurrence cycle	SALT Ksi	Allowable Fatigue Cycle Cycle
PV-01	34.1	192	1.502	Over 1.00 x 1011 Cycle
Slug Catcher	34.2	1344	1.507	Over 1.00 x 1011 Cycle
Inlet Separator	34.3	1728	1.511	Over 1.00 x 1011 Cycle
Nozzle N1	34.4	768	1.516	Over 1.00 x 1011 Cycle
	34.5	960	1.520	Over 1.00 x 1011 Cycle
	34.6	384	1.524	Over 1.00 x 1011 Cycle
	34.7	192	1.529	Over 1.00 x 1011 Cycle
	34.8	192	1.533	Over 1.00 x 1011 Cycle
	34.9	192	1.538	Over 1.00 x 1011 Cycle
PV-01	34.1	192	2.641	Over 1.00 x 1011 Cycle
Slug Catcher	34.2	1344	2.648	Over 1.00 x 1011 Cycle
Inlet Separator	34.3	1728	2.656	Over 1.00 x 1011 Cycle
Nozzle N4	34.4	768	2.663	Over 1.00 x 1011 Cycle

Case	Op. Pressure bar	Occurrence cycle	SALT Ksi	Allowable Fatigue Cycle Cycle
	34.5	960	2.671	Over 1.00 x 1011 Cycle
	34.6	384	2.679	Over 1.00 x 1011 Cycle
	34.7	192	2.687	Over 1.00 x 1011 Cycle
	34.8	192	2.695	Over 1.00 x 1011 Cycle
	34.9	192	2.703	Over 1.00 x 1011 Cycle
PV-02	33.9	192	0.893	Over 1.00 x 1011 Cycle
Prod. Separator	34	1344	0.896	Over 1.00 x 1011 Cycle
Nozzle N4	34.2	1728	0.901	Over 1.00 x 1011 Cycle
	34.3	768	0.904	Over 1.00 x 1011 Cycle
	34.4	960	0.907	Over 1.00 x 1011 Cycle
	34.5	384	0.909	Over 1.00 x 1011 Cycle
	34.6	192	0.912	Over 1.00 x 1011 Cycle
	34.7	192	0.915	Over 1.00 x 1011 Cycle
	34.8	192	0.917	Over 1.00 x 1011 Cycle
PV-03	33.9	192	1.701	Over 1.00 x 1011 Cycle
Amine Contactor	34	1344	1.706	Over 1.00 x 1011 Cycle
Inlet KO Drum	34.2	1728	1.716	Over 1.00 x 1011 Cycle
Nozzle K5B	34.3	768	1.721	Over 1.00 x 1011 Cycle
	34.4	960	1.726	Over 1.00 x 1011 Cycle
	34.5	384	1.731	Over 1.00 x 1011 Cycle
	34.6	192	1.736	Over 1.00 x 1011 Cycle
	34.7	192	1.741	Over 1.00 x 1011 Cycle
	34.8	192	1.746	Over 1.00 x 1011 Cycle
PV-04	33.3	192	7.626	1.50 x 1010 cycle
Amine Contactor	33.4	768	7.648	1.20 x 1010 cycle
Nozzle N4A	33.5	576	7.672	1.20 x 1010 cycle
	33.6	1728	7.694	1.20 x 1010 cycle
	33.7	768	7.718	1.20 x 1010 cycle
	33.8	960	7.740	1.20 x 1010 cycle
	33.9	384	7.763	1.20 x 1010 cycle
	34	192	7.786	1.20 x 1010 cycle
	34.1	192	7.810	1.20 x 1010 cycle
	34.2	192	7.832	1.20 x 1010 cycle
PV-04	33.3	192	1.837	Over 1.00 x 1011 Cycle
Amine Contactor	33.4	768	1.840	Over 1.00 x 1011 Cycle
Nozzle N4C	33.5	576	1.769	Over 1.00 x 1011 Cycle
	33.6	1728	1.774	Over 1.00 x 1011 Cycle
	33.7	768	1.780	Over 1.00 x 1011 Cycle
	33.8	960	1.782	Over 1.00 x 1011 Cycle
	33.9	384	1.790	Over 1.00 x 1011 Cycle
	34	192	1.795	Over 1.00 x 1011 Cycle
	34.1	192	1.801	Over 1.00 x 1011 Cycle
	34.2	192	1.806	Over 1.00 x 1011 Cycle

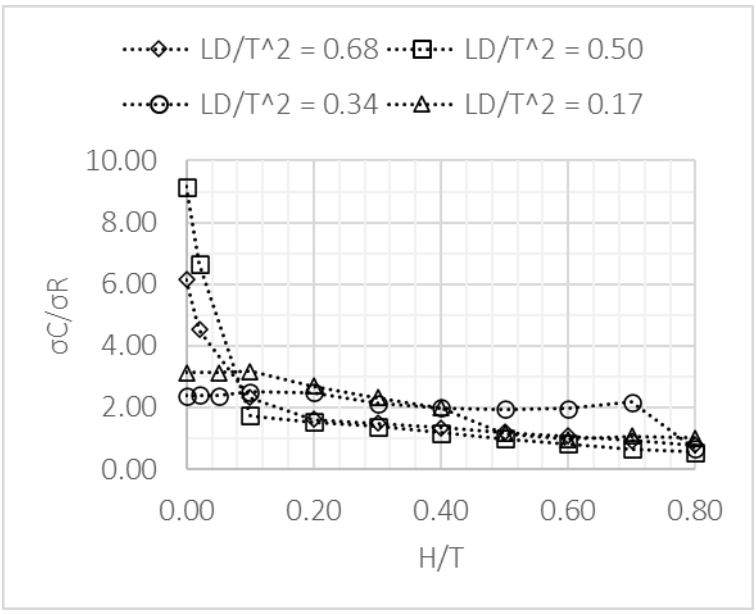

Figure. 9. Stress increase ratio along thickness of plate for surface flaw

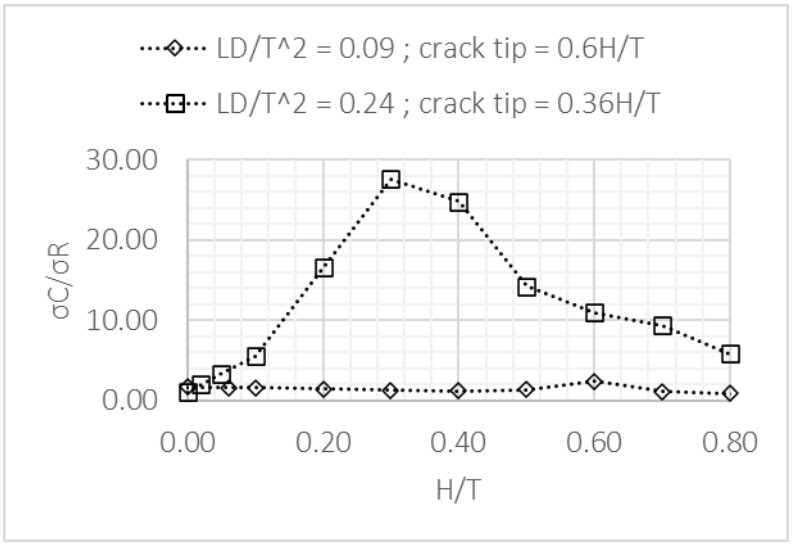

Figure. 10. Stress increase ratio along thickness of plate for embedded flaw

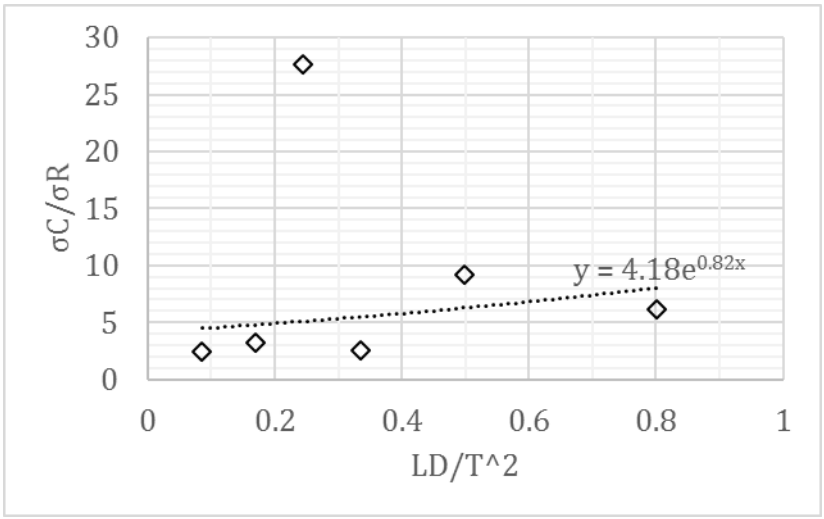

Figure. 11. Correlation between geometry of flaw with stress increase ratio

IV. Discussion

Fitness for service (FFS) assessment for crack-like flaws has been performed based on API Recommended Practice 579-1/ASME FFS-1 Part 9 and has been discussed in the previous section.

Figure 9 and Figure 10 present the stress resulted due to a flaw condition, σ_C, with the reference stress (without flaw), σ_R along the thickness of the shell plate. T represents the thickness of the shell plate; H represents the perpendicular distance between the inner side of the plate to the surface plate at the reference location of the crack tip; D represents the depth of the flaw; L represents the length of the flaw.

For surface typed crack, the stress increase ratio, σ_C/σ_R , are tend to significantly increase near crack tip H/T = 0.0 and gradually decrease and stable approximate the reference stress value at the surface of shell plate, H/T = 0.1 and above. For surface crack, the stress ratio, σ_C/σ_R, tends to significantly increase near crack tip H/T = 0.0 and gradually decrease and stabilize approximate the reference stress value at the surface of the shell plate, H/T = 0.1 and above. For the embedded type flaw, the stress ratio also tends to increase significantly as the reference depth approaches the location of the crack tip. The magnitude of stress increase from surface and embedded typed flaw are affected by crack geometry as presented in Figure 11, the increase of length time to depth of flaw relative to the shell plate thickness, LD/T^2, the higher stress increase will be produced. The correlation between stress ratio with flaw geometry through the exponential function can be used to predict the increase of stress ratio expressed as $\sigma_C/\sigma_R = 4.18e^{0.82(LD/T\text{^}2)}$.

V. Conclusion

Failure assessment include fatigue assessment have been performed for pressurized equipment confirmed with surface and embedded flaws based on the phased array ultrasonic testing survey data. The assessment has demonstrated that the current condition of the deteriorated pressure vessel has adequate strength under operating conditions, furthermore, the fatigue damage is an insignificant factor affecting the life of the equipment. The assessment also shows that the flaw geometry affects the stress increase, the increase in depth and length of the flaw will significantly increase the stress. To maintain safety in the operation of deteriorated pressurized equipment shall be:

a. Maintain their operation pressure in order to not exceed about 56% of the maximum working pressures (MAWP),
b. Perform inspection, monitoring, and testing, and the assessment shall be performed periodically based on API 510 and API 580 to ensure the integrity of the equipment. In addition, and
c. Re-setting the pressure safety valve (PSV), if required.

Acknowledgements

This study was supported by PT. Dinamika Teknik Persada for providing the data set, tools, and funding is gratefully acknowledged.

Conflict of Interest

No Potential conflict of interest was reported by the author.

References

[1] Maurice Stewart. “Surface Production Operations: Volume 5: Pressure Vessels, Heat Exchangers, and Aboveground Storage Tanks: Design, Construction, Inspection, and Testing”. Gulf Professional Publishing, 2021.
[2] American Society of Mechanical Engineers (ASME). “Boiler and Pressure Vessel Code, Section VIII: Rules of Construction of Pressure Vessel”, 2023.
[3] American Petroleum Institute (API). “API 510: Pressure Vessel Inspection Code: In-service Inspection, Rating, Repair and Alteration, 11th Edition”. 2022.
[4] American Petroleum Institute (API). “API Recommended Practice 580: Risk Based Inspection 4th Edition”. 2023.
[5] American Petroleum Institute (API). “API 579-1/ASME FFS-1: Fitness for Service 4th Edition”. 2021.
[6] M. Ghanbari, M.J. Ranjbar Naserabadi and F. Mirzadeh. “Evaluation of a pressure vessel using failure analysis diagram based on phase array ultrasonic testing data”. Journal of Structural Integrity and Maintenance 2022, Vol. 7, No. 3, 198-205.
[7] American Petroleum Institute (API). “API 579: Recommended Practice for Fitness for Service”. Washington DC, 2000
[8] British Energy. “British Energy R-6: Assessment of the integrity of structure containing defect”. 1999
[9] British Standard Institute. “BSI 7910: Guide on method for assessing the acceptability of flaw in structure”. 1999
[10] Ted L. Andreson and David A. Osage. “API 579: A Comprehensive Fitness for Service Guide”. International Journal of Pressure Vessel and Piping, 77 (2000) 953-963.
[11] David A. Osage. “Fatigue Assessment for In-Service Component – A New part for API 579-1/ASME FFS-1 Fitness for Service”. Procedia Engineering 133 (2015) 320-347.
[12] American Petroleum Institute (API). “API 579-1/ASME FFS-1: Fitness for Service 3rd Edition”. 2016
[13] Junk-Suk Lee, Jung-Bog Ju, Jae-il Jang, Woo-Sik Kim, Dongil Kwon. “Weld Crack assessment in API X65 pipeline: failure assessment diagram with variations in representative mechanical properties”. Material Science and Engineering A 373 (2004) 122-130.
[14] Sebastian Cravero, Claudio Ruggieri. “Structural integrity analysis of axially cracked pipeline using conventional and constraint-modified failure assessment diagrams”. International Journal of Pressure Vessel and Piping 83 (2006) 607-617.
[15] S.T. Lie and T. Li. “Failure pressure prediction of a cracked compressed natural gas (CNG) cylinder using failure assessment diagram”. Journal of Natural Gas Science and Engineering 18 (2014) 474-483.
[16] Macros A. Bergant, Alejandro A. Ywny, Juan E. Perez Ipina. “Failure Assessment Diagram in Structural Integrity Analysis of Steam Generator Tubes”. Procedia Materials Science 8 (2015) 128-123.
[17] W. Wu, G.X. Cheng, Y. Li, Q. Zhou, H.J. Hu. “Failure Assessment of cracked pipes based on failure assessment diagram considering random and Fuzzy uncertainties”. Procedia Engineering 130 (2015) 1298 – 1310.
[18] R.A. Ainsowrth, M. Gintalas, M.K. Sahu, J. Chattopadhyay, B.K. Dutta. “Application of failure assessment diagram methods to cracked straight pipes and elbows”. International journal of pressure vessels and piping 148 (2016) 26 – 35.
[19] G, Pluviange, O. Bouledroua, M. Hadj Meliani, Rami Suleiman. “Corrosion defect analysis using domain failure assessment diagram”. International journal of pressure vessel and piping 165 (2018) 126 – 134.
[20] Bassam Gamal Nasser Muthanna, Omar Bouledroua, Madjid Meriem-Benziane, Mahdi Razavi Setvati, Milos B. Djukic. “Assessment of corroded API 5L X52 pipe elbow using modified failure assessment diagram”. International journal of pressure vessels and piping 190 (2021) 104291.
[21] Tsutomu Iwashita, Yoshiaki Kurobane, Koji Azuma, Yuji Makino. “Prediction of brittle fracture initiating at ends of CJP groove welded joint with defect: study into

applicability of failure assessment diagram approach". Engineering Structure 25 (2003) 1815-1826.

[22] Z.M. Yang, S.T. Lie, W.M. Gho. "Failure assessment of cracked square hollow section T-Joints". International Journal of pressure vessel and piping 84 (2007) 244-255.

[23] S.T. Lie, Z.M. Yang, W.M. Gho. "Validation of BS7910:2005 failure assessment diagram for cracked square hollow section T-, Y- and K-joints". International Journal of Pressure Vessel and Piping 86 (2009) 335-344.

[24] Xudong Qian. "Failure Assessment diagram for circular hollow section X- and K-joints". International journal of pressure vessels and piping 104 (2013) 43 – 56.

[25] Aziz Ahmed and Qudong Qian. "A deformation limit based on failure assessment diagram for fatigue-cracked X-joint under in-plane bending". Ships and offshore structure, 2016, Vol. 11, No. 2, 182 – 197.

[26] V. Madrazo, S. Cicero, T. Gracia. "Assessment of notched structural steel components using failure assessment diagram and the theory of critical distances". Engineering failure analysis 36 (2014) 104 – 120.

[27] S. Cicero, V. Madrazo, T. Gracia. "On the assessment of U-shaped notched using failure assessment diagram and the line method: experimental overview validation". Theoretical and applied fracture mechanic 80 (2015) 235 – 241.

[28] S. Cicero, T. Gracia, V. Madrazo. "Structural integrity analysis of notched ferritic steel operating within their ductile to brittle transition zone: an approach from failure assessment diagram and the notch master curve". Engineering failure analysis 58 (2015) 134 – 148.

[29] Jiangchao Zhu, Mauro Madia, Michael Schurig, Bernard Fedelich, Harmut Schlums, Uwe Zerbst. "Brust speed assessment of aero-engine turbine disk based on failure assessment diagram and global stability criterion". Engineering fracture mechanic 277 (2023) 109005.

[30] Giorgio Donzella, Candida Petrogalli. "A failure assessment diagram for component subjected to rolling contact loading". International journal of fatigue 32 (2010) 256 – 268.

[31] G. Donzella, C. Petrogalli and A. Mazzu. "Application of failure assessment diagram under rolling contact with hardness variable along the depth". Procedia engineering 10 (2011) 746 – 751.

[32] Giorgio Donzella, Angelo Mazzu. "Extension to finite life of failure assessment diagram for contact fatigue loading". International journal of fatigue 44 (2012) 217 – 224.

[33] Douglas A. Scarth, Ted Smith. "The use of failure assessment diagram to describe delayed hydride cracking initiation at a blunt flaw". International Journal of pressure vessel and piping 79 (2002) 233-243.

[34] C.M. Davies, N.P. O'Dowd, D.W. Dean, K.M. Nikbin, R.A. Anisworth. "Failure assessment diagram analysis of creep crack initiation in 316H stainless steel". International journal of pressure vessel and piping 80 (2003) 541 – 551.

[35] S. Jallouf, K. Casavola, C. Pappalettere, G. Pluvinage. "Assessment of undercut defect in a laser welded plate made of Ti-6Al-4V titanium alloy with probabilistic domain failure". Engineering failure analysis 59 (2016) 17 – 27.

[36] F.T. Ibanez-Guiterrez, S. Cicero. "Fracture assessment of notched short glass fibre reinforce polyamide 6: an approach from failure assessment diagram and the theory of critical distance". Composite part B 111 (2017) 124 – 133.

[37] Macros A. bergant, Alejandro A. Ywny, Juan E. Perez Ipina. "A comparison of failure assessment diagram option for Inconel 690 and incoloy 800 nuclear steam generator tubes". Annals of nuclear energy 140 (2020) 107310.

[38] Sergio Cicero, Victor Martinez-Mata, Marcos Sanchez, Sergio Arrieta. "Analysis of additively manufactured PLA containing notched using failure assessment diagrams". Procedia Structural integrity 42 (2002) 18 – 26.

[39] S. Cicero, M. Sanchez, V. Martinez-Mata, S. Arrieta, B. Arroyo. "Structural integrity assessment of manufactured ABS, PLA and graphene reinforced PLA notched specimen combing failure assessment diagram and the theory of critical distance". Theoretical and applied fracture mechanic 121 (2022) 103535.

[40] Sergio Cicero, Sergio Arrieta, Marcos Sanchez, Laura Castanon-Jano. "Analysis of additively manufacture notched PLA plates using failure assessment diagrams". Theoretical and applied fracture mechanic 125 (2023) 103926.

[41] Hongzhou Yan, Huayan Chen, Maobing Shuao, Xiangguo Zeng, Bin Huang. "Thermal stresses of large-dimension of lithium hydride ceramic during the sintering process and strength analysis based on process-based failure assessment diagram". Ceramics international 50 (2024) 3930 – 3939.

[42] T.L. Andrson. "Fracture Mechanic: Fundamental and Application – Third Edition". CRC Press Taylor & Francis Group. 2005

[43] Vishal Metha. "Evaluation of the Fracture Parameter for SA 516 Grade 70 Material". IOSR Journal of Mechanical and Civil Engineering (ISOR-JMCE) Volume 13, Issue 3 Ver. III (May-June. 2016), PP 38-45.